fluids

MDPI

Article

Visualization and Quantification of Facemask Leakage Flows and Interpersonal Transmission with Varying Face Coverings

Xiuhua Si [1], Jensen S. Xi [1], Mohamed Talaat [2], Jay Hoon Park [3], Ramaswamy Nagarajan [3,4], Michael Rein [5] and Jinxiang Xi [2,*]

[1] Department of Mechanical Engineering, California Baptist University, Riverside, CA 92504, USA
[2] Department of Biomedical Engineering, University of Massachusetts, Lowell, MA 01854, USA
[3] Department of Plastics Engineering, University of Massachusetts, Lowell, MA 01854, USA
[4] Fabric Discovery Center, University of Massachusetts, Lowell, MA 01854, USA
[5] Advanced Functional Fabrics of America, Cambridge, MA 02139, USA
* Correspondence: jinxiang_xi@uml.edu; Tel.: +1-978-934-3259

Abstract: Although mask-wearing is now widespread, the knowledge of how to quantify or improve their performance remains surprisingly limited and is largely based on empirical evidence. The objective of this study was to visualize the expiratory airflows from facemasks and evaluate aerosol transmission between two persons. Different visualization methods were explored, including the Schlieren optical system, laser/LED-particle imaging system, thermal camera, and vapor–SarGel system. The leakage flows and escaped aerosols were quantified using a hotwire anemometer and a particle counter, respectively. The results show that mask-wearing reduces the exhaled flow velocity from 2~4 m/s (with no facemask) to around 0.1 m/s, thus decreasing droplet transmission speeds. Cloth, surgical, and KN95 masks showed varying leakage flows at the nose top, sides, and chin. The leakage rate also differed between inhalation and exhalation. The neck gaiter has low filtration efficiency and high leakage fractions, providing low protection efficiency. There was considerable deposition in the mouth–nose area, as well as the neck, chin, and jaw, which heightened the risk of self-inoculation through spontaneous face-touching. A face shield plus surgical mask greatly reduced droplets on the head, neck, and face, indicating that double face coverings can be highly effective when a single mask is insufficient. The vapor–SarGel system provided a practical approach to study interpersonal transmission under varying close contact scenarios or with different face coverings.

Keywords: face covering; mask fit; leakage flows; Schlieren optical imaging system; interpersonal transmission; self-inoculation; short-range airborne transmission; double masking

Citation: Si, X.; Xi, J.S.; Talaat, M.; Park, J.H.; Nagarajan, R.; Rein, M.; Xi, J. Visualization and Quantification of Facemask Leakage Flows and Interpersonal Transmission with Varying Face Coverings. *Fluids* **2024**, *9*, 166. https://doi.org/10.3390/fluids9070166

Academic Editors: Markus Klein, Mingming Ge, Xin-Lei Zhang and Guangjian Zhang

Received: 4 June 2024
Revised: 4 July 2024
Accepted: 13 July 2024
Published: 22 July 2024

1. Introduction

Proper fit is crucial for the safety, comfort, and functionality of face masks [1,2]. Recent advancements have greatly improved filter media, enhancing aerosol filtration efficiency while maintaining an acceptable pressure drop [3–6]. However, the effectiveness of even the most advanced filter media is compromised if the mask does not fit the wearer properly. Essentially, a mask only functions as personal protective equipment if air flows through the filter media and not around it through gaps between the mask and the skin [7]. Consequently, the protective level of the mask directly correlates with the amount of air leakage [8]. A poor fit can dramatically decrease a mask's overall protection efficacy. Notably, unlike tight-fitting respirators, disposable three-layer surgical masks often have a loose fit that can worsen during physical activities, incorrect usage, or extended wear [9–13].

Gaps between a mask and skin can significantly affect airflow and aerosol movement, depending on their size and location. However, current standardized tests cannot measure these gaps or link them to mask fit. While mask-fit testers exist for tight-fitting respirators, similar tools for loose-fitting masks, like disposable surgical masks, are lacking [14–19]. For instance, directly applying the TSI Portacount mask-fit tester to surgical masks yields

unrealistically low scores (0–40) with large variability. Also, while we can measure air speed through gaps, measuring gap size is difficult. These gaps change with activity, face shape, and facial hair. Wang et al. showed that nose height and chin length notably influenced the leak site in loose-fitting masks [20]. In a similar manner, Oestenstad et al. showed that the leak site changed with the face size and shape [21]. Even gender and age matter—women often have leaks at the mask's bottom [22]. Overall, accurately measuring mask leakage is still challenging, and leakage testing should use anatomically accurate or even sub-specific face models [20,23–25].

Previous studies have explored different methods to characterize mask flows, especially leakage flows and escaping particles. Using a Schlieren optical imaging system, Tang et al. found that while surgical masks block a cough's forward jet, a poor fit can allow for air leakage from the top and sides [26]. Similarly, Su et al. reported comparable reductions in filtration efficiency among various loose-fitting masks (cloth, surgical, and KN95) against ultrafine particles [27]. Cappa et al. measured exhaled aerosols using a particle sizer and showed that imperfect sealing in surgical masks significantly reduced their ability to block expiratory particles during talking and coughing [28]. Koh et al. simulated exhalation and coughing in a manikin with different masks. Interestingly, they demonstrated that poorly fitting N95 respirators may offer less protection than a simple surgical mask [29]. Also using a manikin model, Brooks et al. demonstrated that knotting the mask band and tucking in the extra material of a surgical mask effectively improved mask fit and protection [30]. Verma et al. utilized a manikin, foot pump, smoke generator, and a laser sheet to visualize a 'cough' through different masks [31]. The team was able to identify sites of leakage in the masks and determine how far the 'cough' traveled after passing through the masks [31]. For normal breathing, the foot pump delivers 500 mL of air to the model per breath, while for coughing, the foot pump delivers 1500 mL, mimicking the average amount of air expelled during a cough [32].

Despite valuable insights obtained from previous visualization studies, they were limited to qualitative analysis and a single test participant wearing a mask. Moreover, the visualization results predominantly focused on exhalation flows. Due to ethical issues, the visualization methods with human subjects had to be safe, and many alternative optical approaches, such as laser-based methods, had to be excluded. The manikin models used in mask flow visualization were often for general purposes, with not-so-accurate facial morphologies. Even more significant, research on interpersonal droplet transmission is severely lacking, even though it is more relevant to evaluating the transmission risks of respiratory infections [33]. One exception was Xu et al., who used a Schlieren system to study the effects of ventilation on airborne aerosol transmission between two persons and suggested that only a sufficiently high personal ventilation can effectively protect against infection [34,35].

The objective of this study is to visualize mask flows and the transmission of respiratory droplets between individuals. Specific aims include the following:

1. Explore different visualization methods for expiratory and inspiratory airflows due to mask-wearing, including systems based on Schlieren, laser, LED, smoke particles, and vapor droplets.
2. Compare facemask flow dynamics under different physical activities and between different mask types.
3. Measure the particle counts and leakage flow rates from different mask types, including cloth, surgical, and KN95.
4. Investigate interpersonal droplet transmission using a vapor-based visualization system between 3D-printed head models under various interaction scenarios.

2. Methods

2.1. Mask Flow Visualization Methods

2.1.1. Schlieren Optical Imaging System

The Schlieren imaging system visualizes airflows by capturing light refraction changes between areas of differing pressure or temperature. This study used a single-mirror setup (Figure 1a) with four parts: a concave mirror (AD015, 406 mm diameter, 1.8 m focal length, Agena AstroProduct, Cerritos, CA, USA), a pinhole LED light source 3.6 m away, a razor blade, and a Canon EOS Rebel T7 camera (Canon, Tokyo, Japan). The mirror reflects light through the test area to the razor, which blocks half the light. The remainder reaches the camera, producing an image. Dimmed lighting enhances airflow visibility. Image sensitivity depends on the mirror's focal length to unobstructed object length ratio [36]. During the test, the participant sat 20 cm from the mirror, with or without face coverings, as illustrated in the rightmost panel in Figure 1a. Five activities were performed: normal breathing, coughing, soft speaking, normal breathing, and loud speaking, that represented the majority of everyday activities. For normal breathing, the effect of a bracket on mask flows was also tested. Four types of masks were evaluated in this study, including a surgical mask (JS95-01, SanJiao, KN95 (EVENTRONIC., Shenzhen, China, with a filtration efficiency of 99.1% and a breathability of 168 Pa)), cloth mask (Newmark Sports, Irvine, CA, USA), and neck gaiter (Finvizo). According to assessments by the National Personal Protective Technology (NPPTL), the JS95-01 surgical mask has a filtration efficiency of 82.4–89.0% and breathability of 71–107 Pa (test #: MTT-2020-104.1), and the EVENTRONIC KN95 has a filtration efficiency of 93.3–99.6% and a breathability of 160–206 Pa (test #: MTT-2021-57.1) [37]. The filtration efficiency and breathability of the cloth mask and neck gaiter were not measured.

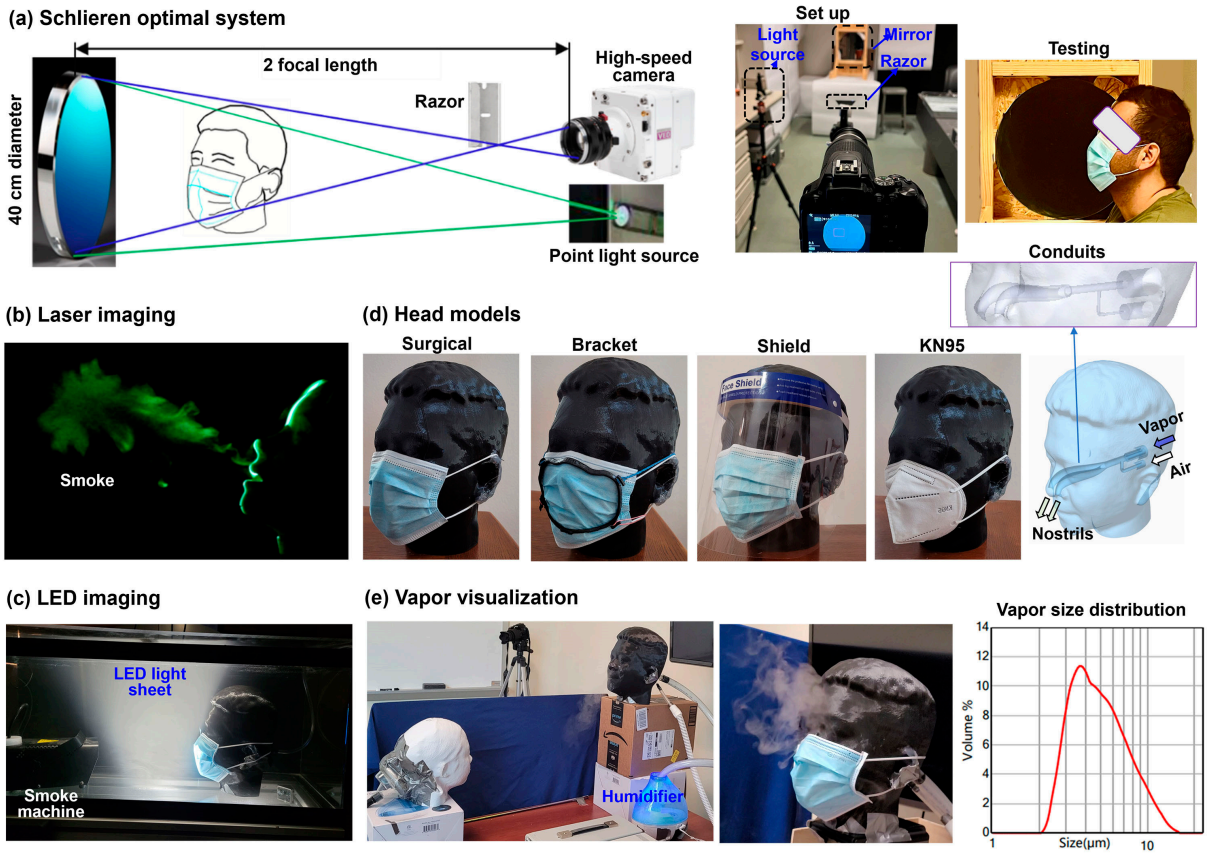

Figure 1. Experimental methods: (**a**) Schlieren optical imaging, (**b**) laser imaging, (**c**) head models with various face coverings, (**d**) LED imaging, and (**e**) vapor-based visualization.

2.1.2. Laser-Particle Imaging System for Exhalation

The laser system was created using a laser sheet, a head model, a foot pump, and a fog machine. A laser sheet (100 mW, 488 nm) was used to illuminate expiratory flows that contain fog particles (Figure 1b). The foot pump was used to pump a puff of air through the head model, simulating the way air is quickly released from the nose/mouth during coughing or breathing. A fog machine (CHAUVET DJ Hurricane 1000, Antwerpen, Belgium) was used to create tracer particles. The laser sheet was pointed toward the respiratory model to create a midsagittal cross-section of the expelled smoke. All testing was conducted in a dark room so that the illuminated particle-laden flows could be clearly visible. All testing was recorded using the same camera that was used for the Schlieren system images.

2.1.3. LED-Particle Imaging System for Inhalation and Exhalation

Considering that the foot pump could only generate expiratory flows, another visualization system was designed that allowed for the visualization of both inhalations and exhalations. To visualize the inspiratory flows that flow inwardly into the nose/mouth, seed particles need to be present outside the head model before inhalation. Ideally, these seed particles should be evenly suspended and as still as possible so that when inhalation starts, the particle trajectories converging toward the mouth/nose or mask can be sufficiently different from the surroundings. To achieve this, a 50-gallon fish tank was used, which was pre-filled with fog smoke five minutes before the test to allow for the fog particles to stabilize (Figure 1c). An LED sheet light was used to illuminate the mid-sagittal plane of the head model. A breathing machine was used to ventilate a sinusoidal pressure waveform to the head model, and the same camera that was used for the Schlieren imaging was used to record the flow dynamics around the mask (Figure 1c). Note that, even for exhalation, this LED-fish tank system is different from the laser–foot pump system described in Section 2.1.2 in that it visualizes how the ambient air is disturbed by expiratory flows, while the laser system visualizes how the exhaled particles are dispersed in the environment.

2.2. Quantitative Measurements of Flows, Temperature, and Particles

2.2.1. Leakage Flow Velocity and Mask Temperature

The velocity of leakage flows was measured using a TSI 9565 VelociCalc ventilation meter (Shoreview, MN, USA). Considering that the flow would decay as it moved away from the gap, the probe was positioned 2 cm from the gap sites for all tests. The sites selected for velocity measurement included two nose top ridges, two lateral sides, and the chin, based on prior observations of leakage flows of different masks. When conducting the tests, the participant wore a mask with a good fit and breathed naturally. Each test was repeated five times. Considering that the measured velocity magnitude could vary slightly even for the same leakage site depending on the probe location, the probe was positioned approximately 2 mm away from the center of the gap for all tests. Meanwhile, the mask temperature was recorded with a FLIR ONE Pro iOS thermal camera (Wilsonville, OR, USA).

2.2.2. Particle Counter Testing

A Temtop PMD 331 Particle Counter (Temtop, San Jose, CA, USA) was used to measure the number of droplets exhaled across the mask during normal breathing, as well as the size of each of the droplets. This particle counter can detect aerosol droplets from 0.3 μm to 10 μm in size and has seven channels. The SARS-CoV-2 virus is around 0.1 μm, which can escape mask filtration [38]. However, viruses typically attach to larger droplets or particles to survive and spread, ranging from 0.3 μm to large drops of several millimeters [39]. In addition to the control case (no mask), six types of masks were tested: surgical, KN95, cloth, cloth with HEPA filter, neck gaiter, and surgical with bracket. The tests were conducted in a controlled environment at 24 °C and 30% relative humidity. An air purifier was operated

for one hour prior to testing to ensure that the majority of droplet particles detected by the particle counter came from breathing.

2.3. Head Models

Several head models were used in this study. One was the respiratory model (Michigan Instruments, Grand Rapids, MI, USA) that allowed for air to be expelled through the mouth only. The other two head models were developed from scans of two volunteers using the iPhone app Bellus3D (Lilburn, GA, USA). The use of human scans in this study has been approved by the Institutional Review Board (IRB) of the University of Massachusetts Lowell. The head model was further processed using SolidWorks (Dassault Systèmes, Waltham, MA, USA) to add two conduits, with one connecting to a breathing simulator (Michigan Instruments, Grand Rapids, MI, USA) and the other to a vapor source (rightmost panel, Figure 1d). The head models were manufactured using a Dimension 1200es 3D printer and ABS printing material (Stratasys, Eden Prairie, MN, USA). Due to its life-size and accurate facial topology, the head model can adequately simulate the mask's fit to the face, as demonstrated in Figure 1d.

2.4. Interpersonal Transmission Visualization System

To investigate interpersonal droplet transmission, two head models were placed at a specified distance and relative height (Figure 1e). The head orientation of the two head models could also be adjusted as needed. Each head model was ventilated to a breathing simulator with a sinusoidal waveform (Michigan Instruments, Grand Rapids, MI, USA). The source head model (black color, Figure 1e) was also connected to the vapor source to simulate exhaled droplets, while the recipient model (white color, Figure 1e) was only ventilated with tidal air flows. An ultrasonic humidifier (Pure Enrichment, Huntington Beach, CA, USA) was used to generate soft mist. A SprayLink laser diffraction spray particle size analyzer (Dickinson, TX, USA) was used to measure the size distribution of the soft mist exhaled from the head model without a mask under constant expiratory flows [40]. As shown in Figure 1e, the size distribution was 2.64, 3.92, and 8.51 µm for D10, D50, and D90, respectively. This size range is close to that of expiratory droplets from deep lungs [41–43]. During testing, the ambient temperature was 24 °C and the relative humidity was 31%.

2.5. Numerical and Statistical Methods

2.5.1. Computational Fluid Dynamics (CFD) Simulations

Complementary CFD modeling and simulations were performed. An integrated mask-wearing model was developed that included the ambient air, facemask, face geometry, and airway. Gaps at the mask–face interface were modeled using individual volumes of the mask filter medium that had the properties of air rather than a porous medium. More details of the computational model, along with the mesh generation and grid-independent study, were provided in [44,45]. The computational domain consisted of three volumes: ambient air, mask, and nose–mouth–throat airway. The ambient air and airway were defined as airflow regions, while the mask was modeled as a porous medium. Darcy's law was applied to calculate the viscous resistance (R) of the mask filter, i.e., $R = \Delta P/[(Q/A)\cdot \mu L]$, with ΔP being the breathing resistance, Q the volume flow rate during the mask test, A the test area, μ the air dynamic viscosity, and L the mask thickness. For a surgical mask, the resistance ΔP was measured to be 14.6 mmH_2O using a 8130A Automated Filter Tester (TSI, Shoreview, MN, USA), the flow rate Q was 80 L/min, the test area A was 45.6 cm^2, the flow viscosity μ was 1.825×10^{-5} kg/m·s, and the mask thickness L was 2.3 mm, leading to a viscous resistance of 3.727×10^9 $1/m^2$ [45]. Steady exhalations were considered, with a constant positive pressure being specified at the trachea opening and zero pressure in the far field of the ambient air. Air temperatures were set at 37.15 °C in the airway and 24 °C in the environment. The low-Reynolds number (LRN) k-ω turbulent model was utilized to

simulate the multi-regime flow dynamics. ANSYS Fluent 23 (Canonsburg, PA, USA) was used to solve conservation equations for mass, momentum, and energy.

2.5.2. Statistical Analysis

Minitab 21.4 (State College, PA, USA) was applied to analyze the leakage flow velocities and cross-mask particle counts. A one-way analysis of variance (ANOVA) was used to evaluate the variability of the measurements. A p-value < 0.05 indicated statistical significance difference.

3. Results

3.1. Control Cases

3.1.1. Schlieren Optical Imaging System

Figure 2 shows the Schlieren visualization results of the exhaled flows from a participant with different masks, i.e., surgical, KN95, cloth, and neck gaiter (N-Gaiter). For each mask, five activities were tested: normal breathing, coughing, soft speaking, normal speaking, and loud speaking. The effects of wearing a mask bracket were also evaluated for all masks except the neck gaiter. Considering that a good mask should distribute airflow over the mask and seal well, the mask performance was evaluated qualitatively based on how much air is seen escaping the mask and where leakages are occurring. For all masks tested, the KN95 mask was found to have the least amount of air escaping from the mask for all activities. By comparison, the cloth, surgical, and neck gaiter exhibited large amounts of air escaping from the tops/sides of the mask, as well as through the mask filter material itself. The jet-like flows through the cloth mask and neck gaiter are due to the larger fiber pores that allow for air to pass through them more freely, while the KN95 mask has smaller filter pores. This makes it more difficult for airflows and particles to pass through and helps distribute the airflow all over the mask, thus lowering the exhaled flow speed crossing the mask and extending the effective filtration area.

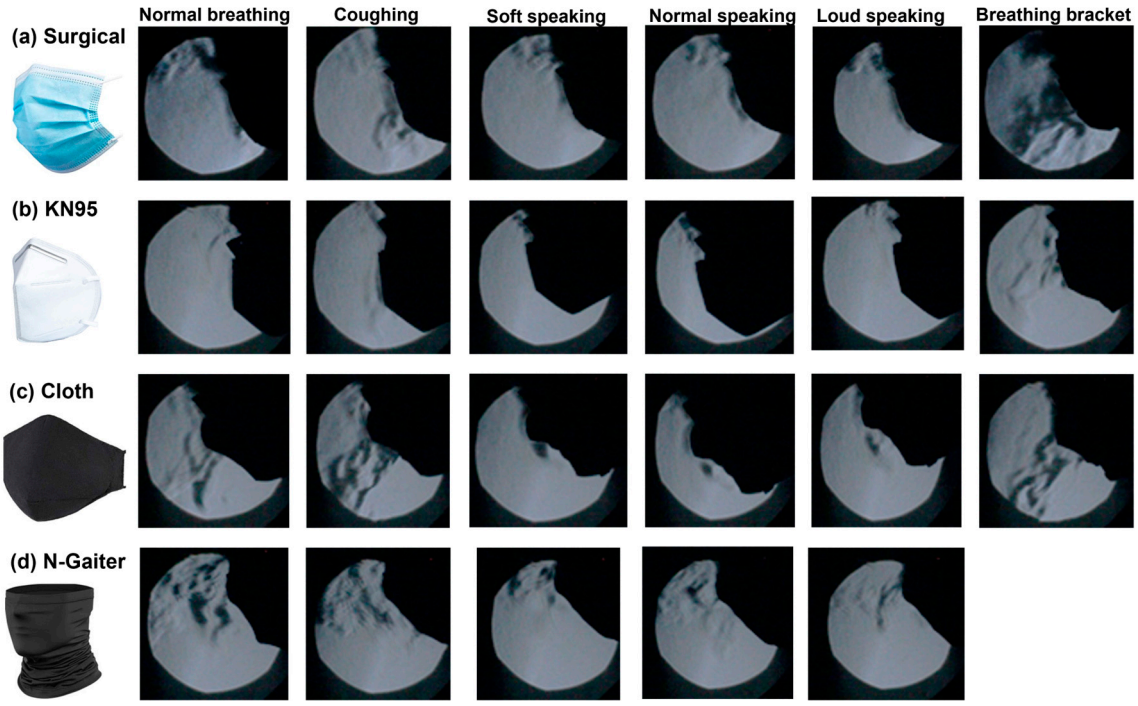

Figure 2. Representative Schlieren imaging (from multiple tests) of expiratory mask flows under various activities from a participant: (**a**) surgical mask, (**b**) KN95, (**c**) cloth mask, and (**d**) neck gaiter. Test activities include normal breathing, coughing, soft speaking, normal speaking, loud speaking, and breathing with a bracket.

Considering the three speaking scenarios (i.e., soft, normal, and loud, Figure 2), no apparent jet flows were observed through the masks, primarily because of the intermittent flow pulses during speaking, regardless of the speaking volume. When a mask bracket was used (last column, Figure 2), intensified jet flows were observed crossing the KN95 and surgical masks, as the bracket effectively confined the exhaled flows within the boundary of the bracket. The purpose of a mask bracket is to fit the mask to the face better, specifically with surgical masks that can create gaps at the sides of an individual's face.

For a given mask, we observed similar flow patterns among different activities, whether the test subject was breathing, coughing, or speaking at different volumes. This demonstrated the mask's overall consistency in effectively containing exhaled airflows under different physical activities. However, differences in flow patterns were also observed among various activities. For example, with the cloth mask (Figure 2c), coughing produced a jet flow across the mask, whereas this jet flow was absent during speaking, regardless of intensity (i.e., soft, normal, or loud). Note that the considered activities have very different dynamics, where breathing releases air constantly from the nostrils, coughing releases air from the mouth quickly at high pressure, and speaking releases air intermittently from the mouth. Moreover, the latter two activities also involve the motion of the mouth, particularly the lips, which may affect the mask fit.

3.1.2. Laser Sheet System

Figure 3 shows the laser visualization of expiratory mask flows in two head models. It is observed that a breath exhaled from the head model traveled directly forward and dispersed in the air. A commonality among all the masks was leakages out of the top of the mask. In addition, fog particulates were able to pass directly through the cloth mask without a HEPA filter and through the neck gaiter. When the HEPA filter was placed in the cloth mask, there was no passage of fog directly through the mask. This finding highlights the effectiveness of the HEPA filter in improving the effectiveness of cloth masks.

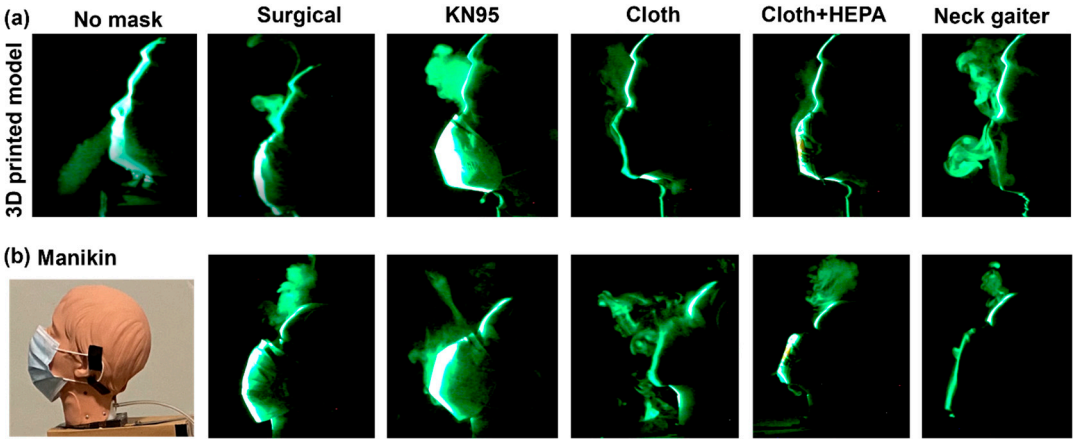

Figure 3. Representative laser visualization (from multiple tests) with different masks on two head models: (**a**) 3D-printed head model and (**b**) manikin.

Considering flows with the 3D-printed model (Figure 3a), leakages occurred at the nose top with the surgical mask, KN95, and the neck gaiter. When comparing the results between the 3D-printed head and the manikin (Figure 3a vs. Figure 3b), one can see that the cloth masks (both with and without the HEPA filter) and surgical mask all performed better with the 3D head model. This is likely due to the 3D head model being larger in size and fitting the masks better than the manikin. These findings demonstrate the importance of proper mask designs for different population groups, such as adults and children.

Based on the findings from the laser sheet experiments, the neck gaiter and the cloth mask without the HEPA filter were less effective in preventing the spread of exhaled air due to their sites of leakage and their inability to distribute the airflow evenly across the filter.

The surgical mask, the cloth mask with the HEPA filter, and the KN95 mask performed better in blocking and spreading the exhaled air despite having leakage through the top of the masks. These leakages highlight the important fact that masks are not 100% effective, necessitating social distancing and hand/face cleaning to mitigate viral transmission.

3.1.3. Particle Count across Various Masks

Figure 4 shows the exhaled particle counts across the masks in total (Figure 4a) and particle size-specific numbers (Figure 4b) for different masks. Large differences in particle counts were observed in Figure 4b between all masks and the no mask control except for the neck gaiter. As expected, the largest number of exhaled droplets was detected with no mask-wearing, followed by the neck gaiter, cloth, surgical with bracket, surgical, cloth with HEPA filter, and KN95 (Figure 4a,b). The slightly higher number of droplets from 'surgical + bracket' than from 'surgical' is because the bracket confined the exhaled flow droplets within the bracket and reduced leakages from the mask–face interface.

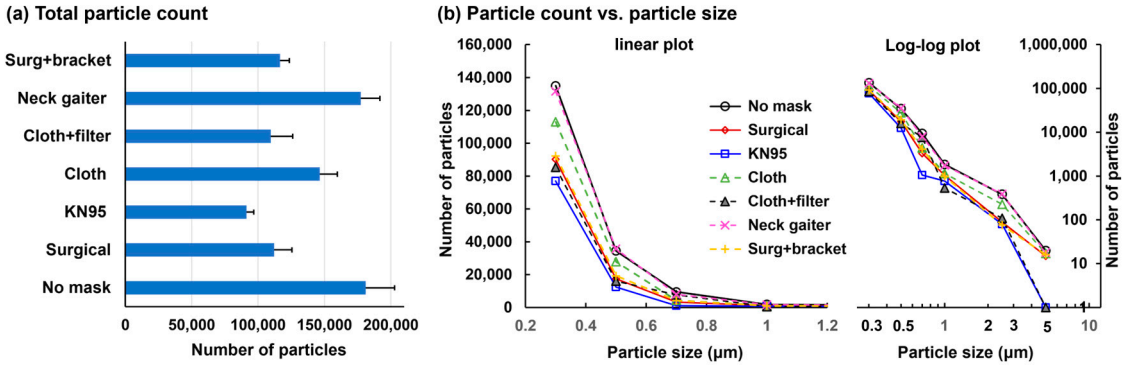

Figure 4. Exhaled particle counts across various masks from a participant: (**a**) total particle count, (**b**) particle count vs. particle size. 'Surg + bracket': Surgical plus bracket.

3.2. Leakage Flow Visualization and Quantification

3.2.1. Leakage Flow Velocity Measurement

Considering that leakages are mostly observed at the nose top and two sides during exhalation, the speeds of the leakage flows were measured using a hotwire anemometer at the right and left ridges of the nose top, two sides, and the chin (Figure 5a).

For the three masks considered (cloth, surgical, and KN95), the leakage flow speeds are much higher from the two ridges than the two lateral sides and chin. Mask-specific differences are also observed, with more leakages from the chin for the cloth and KN95 masks and more lateral leakages from the surgical mask. These observations are consistent with the peculiar mask geometry and its fitting to the facial topology. Both the cloth and KN95 masks have a flat region covering the cheeks, while the surgical mask is tucked up on both sides, forming an arch that allows for leakage flows. Among the three masks, the cloth mask had the highest leakage flow speed (1.7 ± 0.5 m/s, Figure 5b), followed by the surgical mask (1.3 ± 0.5 m/s, Figure 5c) and KN95 (0.24 ± 0.1 m/s. Figure 5d). This difference is also evident by the different ranges in the y-axis among Figure 5b–d. By comparison, the jet flow velocity exhaled from the nostrils without a mask was measured to be 2~4 m/s, while the flow velocity across the mask was 0.1~0.2 m/s.

Figure 6 shows the speeds of the inward leakage flows at different sites during inhalation for three mask types. Note that for both inhalation and exhalation, the mask was carefully pressed to conform to the participant's facial topology as much as possible, thus representing the best scenario of mask fit. The thermal images of the mask are blue in color, indicating the cooling effects from inspiratory ambient air, which contrasts with the warming effect (brown color) from the expiratory air at body temperature (Figure 6a vs. Figure 5a). The overall leakage speeds during inhalation are lower than those during exhalation (Figure 6 vs. Figure 5). This is due to the jet flow features of the expiratory flows

in contrast to the converging flow features of inspiratory flows. Considering the side fitting, inward leakage is not observed in the cloth and KN95 masks (Figure 6b,d) but is observed in the surgical masks (Figure 6c), corroborating the finding that a tucked-up fold is more prone to mask–face gaps and leakage flows.

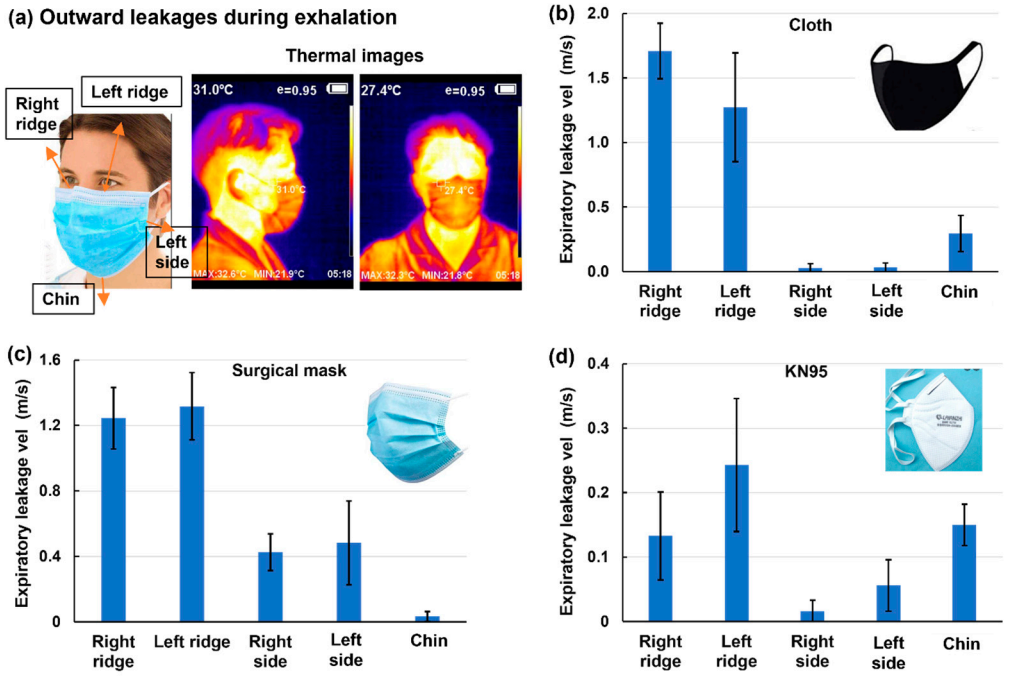

Figure 5. Leakage flow speed measurement during exhalation: (**a**) outward leakage diagram and thermal imaging, (**b**) cloth mask, (**c**) surgical mask, and (**d**) KN95.

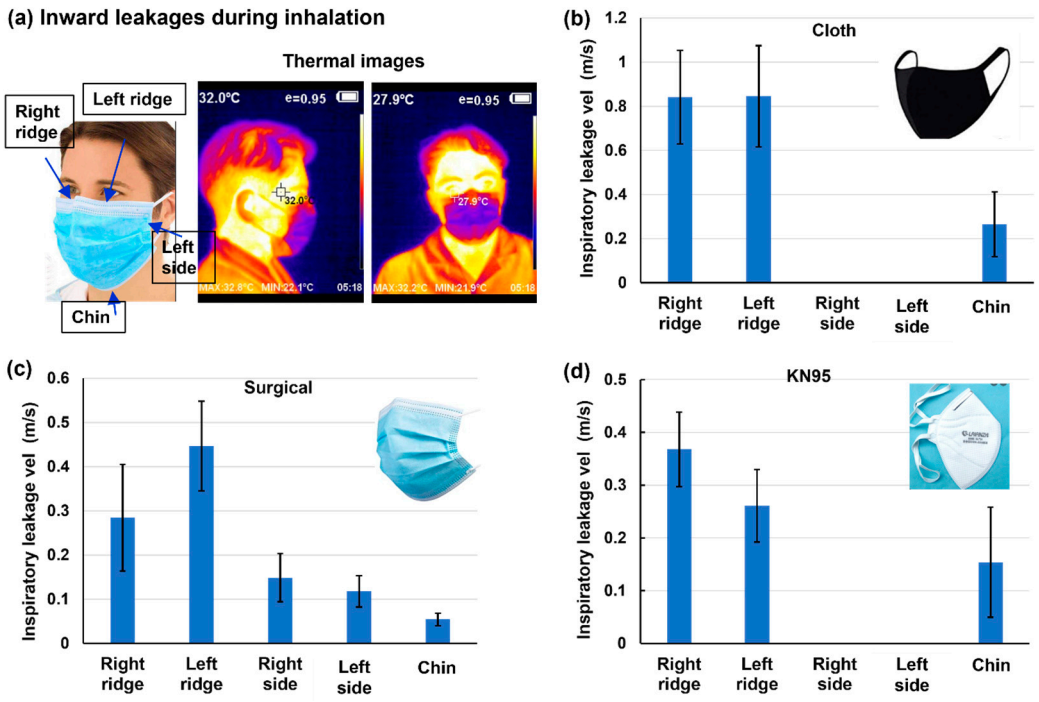

Figure 6. Leakage flow speed measurement during inhalation: (**a**) inward leakage diagram and thermal imaging, (**b**) cloth mask, (**c**) surgical mask, and (**d**) KN95.

3.2.2. In Vitro Visualization vs. CFD

The visualization of mask flows, especially underneath the mask, can provide detailed information on flow, pressure, and temperature to enhance our understanding of facemask dynamics and thermoregulation. Figure 7 compares the experimental (upper panels) and computational (lower panels) results without mask-wearing (Figure 7a), with a surgical mask and side gap (Figure 7b), and with a well-fitted surgical mask (Figure 7c). As shown in Figure 7a, the expiratory jet flows from the nostrils resembled each other between the laser-fog imaging and the predictions from computational fluid dynamics (CFD). The lower panel of Figure 7b displays the inspiratory flow streamlines, which converge from all directions but intensify considerably through the side gap [45,46]. To validate the CFD model, measurement of the flow velocities at the gap was conducted, which agreed favorably with the CFD simulations (Figure 7b).

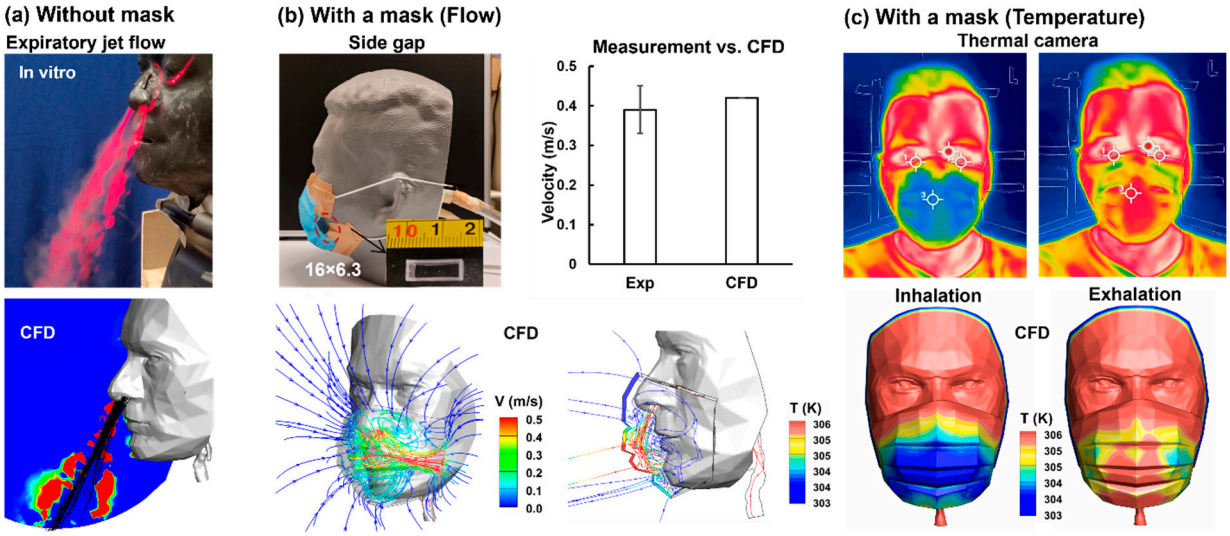

Figure 7. Experiments vs. computational fluid dynamic (CFD) simulations: (**a**) without a mask, (**b**) with a mask for flow, and (**c**) with a mask for temperature.

The lower panel of the third column (Figure 7b) shows the CFD-predicted temperature distribution during exhalation, where the warm jet flows from the nostrils are cooled down and well mixed within the mask–face space. Due to the mask resistance, strong recirculation forms under the mask, eliciting quick mixing. Note the higher temperatures of the mask where the exhaled jet flow impinges compared to other regions of the mask. Figure 7c compares the facial temperature obtained using a thermal camera and complementary CFD simulations. Again, high levels of resemblance are observed between the experiments and CFD for both inhalations and exhalations, further validating the computational model in capturing mask-wearing-associated thermoregulation, which in turn provides thermo-fluid details under the mask that are not easy to measure accurately or non-disruptively. Higher levels of similarity are also observed in comparison to the thermal images in Figures 5 and 6.

3.3. LED-Fog System to Visualize Inhalation–Exhalation Flows

Figure 8 shows the inspiratory and expiratory vector fields in two breathing cycles in a head model wearing a surgical mask. Due to leakages at the nose top, high-speed flows are observed for both inhalation and exhalation cycles. The vectors at the nose top are much longer than the ones in front of the mask. Smoke streaks are observed moving away from the mask, as indicated by the yellow arrows in Figure 8a and red arrows in Figure 8b. These streams advance forward slowly and, at the same time, oscillate due to cyclic inhalation and exhalation, forming complex flow patterns. By contrast, the flows in the immediate proximity of the mask change quickly with the breathing cycle. The slow

advancement of the smoke streaks away from the mask suggests that the exhaled droplets are likely to behave similarly. Thus, the overall advancement speed can indicate whether or when virus-laden respiratory droplets from an infected person reach the recipient at a specific distance.

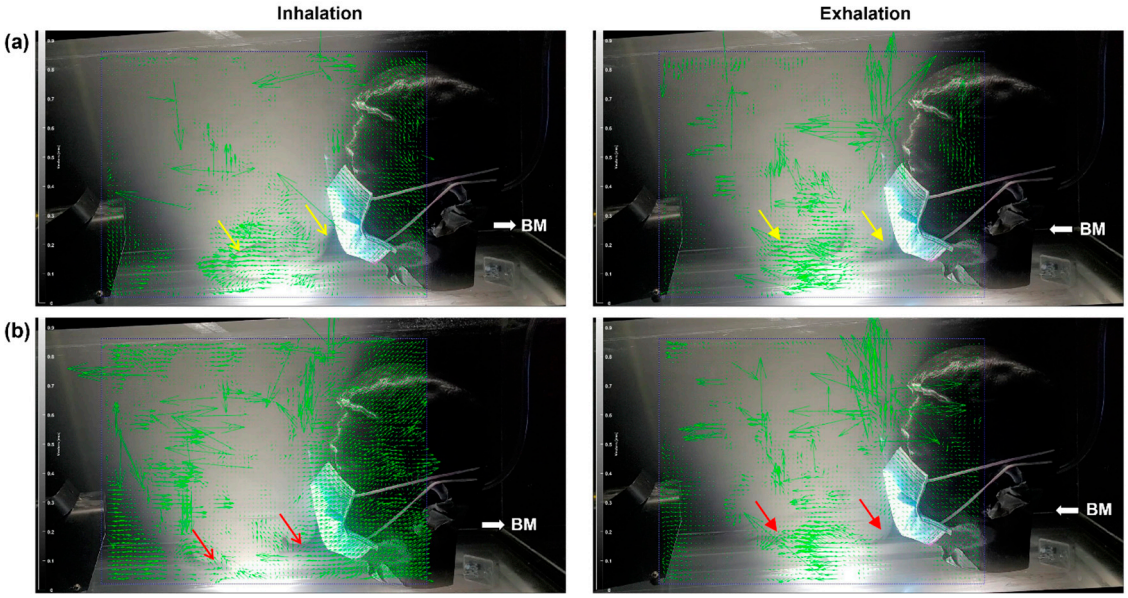

Figure 8. PIVlab analyses of the LED-illuminated smoke distribution during inhalation and exhalation in a head model with a surgical mask over two breathing cycles: (**a**) cycle A and (**b**) cycle B.

3.4. Interpersonal Droplet Transmission

3.4.1. Without Face Covering (1.2 m): The Control

The interpersonal transmission of exhaled droplets is shown in Figure 9 after 5 min of exposure at a distance of 1.2 m between the source and recipient. The droplet deposition is visualized using SarGel, which turns from white to pink upon contacting water, with more deposited water mass correlating with a deeper pink color [47]. The right three panels of Figure 9a,b display different views of the droplet deposition on the head model that is ventilated with a tidal breathing machine. Heterogeneous deposition distributions are observed on the face in both test cases. However, a much-enhanced deposition occurs at the lower cheek (or jaw) and neck (Figure 9b), presumably because the droplet trajectories in the second case are more aligned with the recipient's neck than in the first case.

3.4.2. With Face Covering (1.5 m)

Figure 10 shows the effects of various types of face coverings on interpersonal droplet transmission at a distance of 1.5 m. In both cases, the source wore a surgical mask and a face shield. Thus, the exhaled droplets mainly escaped from the bottom, and a smaller fraction escaped from the two lateral sides of the face shield. Note that none of these three sites pointed to the recipient. The exposure lasted for twenty minutes, and photos of the droplet deposition were taken every five minutes with the mask on and removed. The deposition after 5 min of exposure was negligible in both cases and is thus not presented here.

Two observations are noteworthy regarding the droplet deposition from 10–20 min. First, the progression of deposition is nonlinear with time, which is unnoticeable during 0–5 min, becomes discernable during 5–10 min, but increases quickly between 10 and 20 min (Figure 10a). This suggests that the exhaled droplet plume needs time to propagate from the source to the recipient. However, once the plume reaches the recipient, the deposition will be continuous and become noticeable after a short time, as illustrated by the quick color change from 10 to 15 min. Second, more deposition was observed in the

mouth–nose region and the jaw–neck region. The deposition on the hairs of the frontal head is also notable.

Figure 9. Visualization of interpersonal transmission of respiratory droplets after 5 min exposure when both the source and recipient do not wear a mask: (**a**) both standing or sitting and (**b**) source standing and recipient sitting.

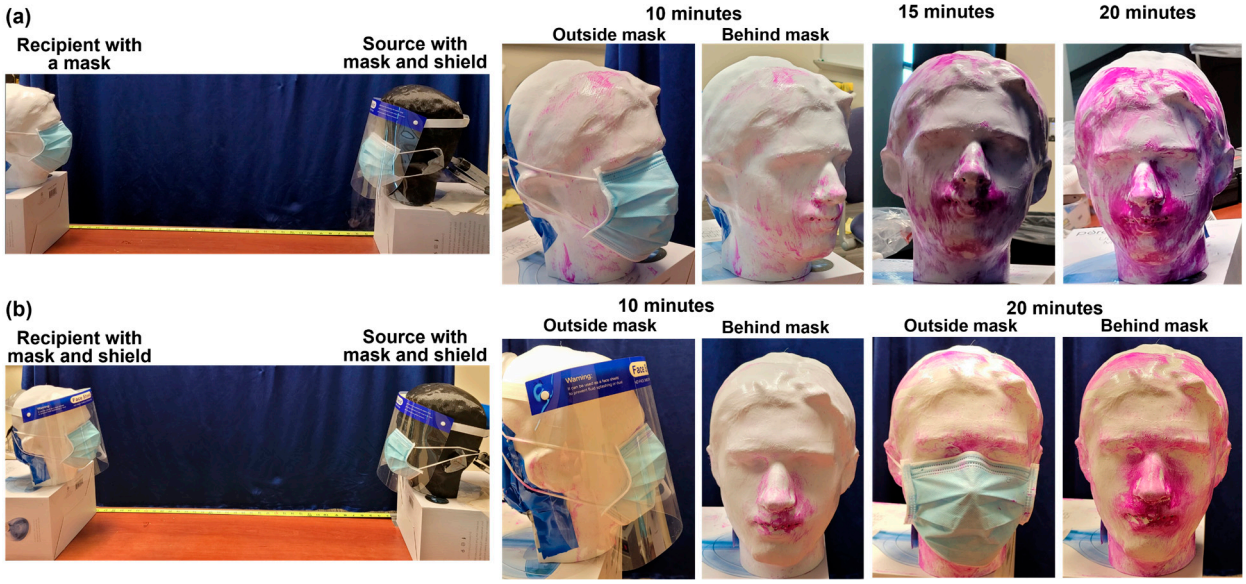

Figure 10. Effects of a face shield on inter-person transmission for varying exposure durations with the source person wearing both a surgical mask and face shield: (**a**) the recipient wearing a surgical mask and (**b**) the recipient wearing a surgical mask and face shield.

Figure 10b illustrates the effects of double protection with the recipient adding a face shield on top of a surgical mask. Compared to wearing a surgical mask only, the face deposition is significantly lower after 10 min of exposure, indicating the effectiveness of extra face-shield protection, which indeed reduced the number of droplets reaching the face underneath the surgical mask. In this case, the droplets need to avoid impacting the face shield by moving downward in front of the shield and subsequently moving upward to reach the mask. This would decrease the leakage flows from the nose top and make more airflow cross the mask filter medium. Wearing a face shield might also have pressed down

the tucked-up arch at two sides, reducing side leakages. Slight deposition in the philtrum region is observed after a 10 min exposure, with no discernable deposition in other regions of the head model (Figure 10b). An additional 10 min of exposure remarkably increased the deposition in the philtrum region, as well as in the nasofacial sulcus, and to a lesser degree, on the nasal ridge and neck (Figure 10b).

4. Discussion

Even though mask-wearing has become ubiquitous, knowledge to quantify its performance or improve its performance is surprisingly limited and empirical at best. This study explored multiple methods to visualize mask-related flows and droplet transmission to better understand mask performance, including the Schlieren optical system, laser imaging system, thermal camera, and vapor–SarGel system. Interesting observations and further thoughts on mask-wearing are discussed below.

4.1. Leakage Flow Characterization

In this study, for all masks considered, leakages from the nose top were observed to be notably higher than those from any other sites (i.e., two lateral sides and chin). Therefore, efforts to improve the mask fit at the nose top are both compelling and rewarding. For instance, using a wider and stronger nasal strap in the surgical mask will not only improve the mask fit to the nose ridge but also help the mask maintain its good fit during various physical activities [48]. A 'Knot-and-tuck' method also promises to achieve a better fit [49]. By knotting the ear loops of a surgical mask and tucking excess material under the edges, a 3D cup-shaped mask forms that better conforms to the facial topology, thus improving the mask–face fit and reducing sideway leakages. It is noted that standardized methods or devices to quantify leakages or fit for disposable masks are lacking, even though commercial devices for tight-fitting respirators are available. One example is the PortaCount Respirator Fit Tester 8038 (TSI, Shoreview, MN, USA); a fit score of no less than 200 under all tested activities is considered a pass. However, when used for loose-fitting disposable masks, such as surgical masks, the fit scores based on the PortaCount Respirator Fit Tester are very low and exhibit large variability (e.g., 0–40). These erroneous readings are mainly due to the device's working principle, which estimates the fit score based on the aerosol concentrations (generated from NaCl-solution) inside and outside the respirator.

For a loosely fit disposable mask, the aerosols will be easily inhaled across the filter medium or through the inward leakage, equalizing the aerosol concentrations inside and outside the mask, losing the good foundation for fit estimation [27]. Furthermore, while wearing a mask diffuses the expiratory flow compared to the jet-like flow without a facemask, the resulting flow is still not isotropic. The variations in leakage velocity among different leaking sites (Figures 5 and 6) reflect both this flow anisotropy and the size differences of the leakage sites. Additional research is needed to quantify the relative contributions of these two factors. A more practical method is to leverage the temperature variations that are dependent on the leakage flow volume [46,50]. Moreover, the periodic temperature variation within one breathing cycle is expected to provide further information on leakage flows, including the leakage volume (gap size) and site, because the cooling effect during inhalation and warming effect during exhalation are highly sensitive to the leakage flow patterns [51–53].

4.2. Droplet Deposition Visualization and Implications

Interpersonal transmission testing with vapor and SarGel provides a practical approach to visualize the transport and deposition of respiratory droplets that are often invisible in life conditions. It is observed that the relative orientation and distance can notably affect the transport and deposition of respiratory droplets (Figures 9 and 10), making it necessary to systematically study these factors to gain a comprehensive understanding of viral transmission and mask protection. Zhang et al. reviewed the close-contact (or short-range) transmission of aerosols between two individuals and highlighted influencing

physical parameters, such as their distance/orientation, body/head motion, exposure duration, and breathing intensity, among others [54]. Zhang et al. also suggested that an exhaled droplet would need at least 0.6 s to reach the receiver at a distance of 1.5 m, based on an expiratory flow velocity of 2.4 m/s (i.e., 1.5 m over 2.4 m/s equals 0.6 s). Note that it can take much longer than 0.6 s for an exhaled droplet to travel from the source to the recipient because the exhaled droplets will quickly slow down within the ambient air. In this study, we observed that it took even longer (i.e., five minutes, Figure 9) for the SarGel on the head model to turn pink under no-mask conditions and ten minutes and more when both the source and recipient were wearing masks (Figure 10). It is reminded that the color change of SarGel with vapor deposition is a gradual process and becomes a darker pink with accumulating deposition. To reach the color depth on the face in Figure 10a, a deposition intensity of 0.24 mg/cm^2 of vapor is needed [55].

One salient feature in vapor droplet deposition with no mask-wearing is the elevated deposition in the neck, chin, and jaw, as displayed in Figure 10b, where the source is standing and the recipient is sitting. This preferential deposition can cause secondary self-inoculation of the recipient's mucous membrane because people spontaneously touch their eyes, cheeks, chin, and mouth, unknowingly [56–58]. According to a study involving 26 students in 2015, a person touched his or her own face 23 times per hour, with around 44% touching the mucous membranes (mouth, nose, and eyes) and 56% touching the non-mucosal areas (chin, cheek, neck, ears, forehead, and hair), with insignificant differences between right and left hands [59]. In a more recent systematic review that considered ten observational studies, facial self-touching per hour was counted as 50.06 ($\pm$47) times [60]. Considering the high deposition in the neck, chin, jaw, and mouth–nose region, hand/face/neck washing is highly recommended to reduce the chance of self-inoculation via spontaneous face-touching.

4.3. Effect of Double Masking

Double masking has been recommended as an extra measure during the COVID-19 pandemic to further curb viral transmission more effectively than wearing a single mask [61]. It can significantly enhance protection against respiratory droplets that may contain viruses, including COVID-19 [62]. This practice involves wearing one mask over another—typically a cloth mask over a surgical mask—to improve the overall fit and filtration capability of the masks [63]. The CDC has noted that this method reduces exposure by 95% when both masks are worn properly [30]. In this research, we evaluated the effect of double masking on interpersonal droplet transmission by comparing the recipient wearing a surgical mask vs. a surgical mask plus a face shield. Adding a face shield led to improvements: (a) prolonged the time when the droplet deposition became noticeable and (b) reduced the overall deposition on the face and neck of the recipient. Adding a face shield resulted in significant improvements in reducing deposition on the recipient, especially on the cheek and neck, even though deposition in the nose–mouth region was still observed (Figure 10b vs. Figure 10a). The time for deposition onset was also prolonged.

There might be two reasons behind these improvements: modified flow-particle dynamics and enhanced surgical mask fit. The presence of the face shield causes airflow and aerosols that approach the wearer to either collide with the shield or divert upwards from beneath the shield. This not only filters out a fraction of aerosols but also lowers their speeds, making it more difficult for these aerosols to be inhaled across the surgical mask. Furthermore, the face shield can also enhance the fit of the surgical mask to the face by pressing down the tucked-up folds, thus minimizing gaps around the edges of the mask. The seal of the face shield at the forehead also reduces the influx of unfiltered air through the nose top. Thus, adding a face shield to a surgical mask can effectively increase the number of barriers against potentially infectious aerosols while introducing relatively minimal extra resistance due to its side opening to the environment. It can be particularly useful in scenarios where higher protection is needed, such as crowded indoor spaces or when interacting closely with others. Also note that double masking is not recommended

with two disposable masks or with two N95 masks, as these combinations do not enhance fit or filtration effectively and can make breathing more difficult [64–66].

4.4. Limitations and Future Studies

The limitations of this study included an unbalanced focus on exhalation flows, the qualitative nature of results, and a limited number of interpersonal and mask-wearing scenarios. Overall, it is easier to visualize the expiratory flows than inspiratory flows both with and without a mask, due to the jet-like exhalation flows vs. the converging inhalation flows (Figure 7a vs. Figure 7b). The latter often have extremely low velocities (i.e., proportional to $1/r^3$), except in the proximity of the nostrils and face–mask gaps (Figures 7b and 8). By contrast, the exhalation core flow has a much higher velocity, penetrates a longer distance, and maintains a large temperature difference relative to the ambient air (Figure 7b). It is unclear, for a mask with given gaps, whether the outward and inward leakage flow rates are the same or not. An accurate answer to this question will affect the estimation of the mask-fit effect on viral source control or receiver protection.

The major limitation of the visualization methods in this study is that they are mostly qualitative. The Schlieren optical system can also be used to visualize interpersonal droplet transport [26,34]. This, however, requires a large concave mirror, whose cost increases drastically with the mirror diameter [67]. By comparison, the vapor–SarGel system developed in this study is low-cost and directly relevant to interpersonal viral transmission. The vapor droplets are measured to be 3.92 μm on average, which is consistent with the respiratory droplets generated in the alveolar region from liquid film ruptures [41–43]. Note that the alveolar region is the major site of SARS-CoV-2 viral infections [68]. Droplets larger than 10 μm were not considered in this study. Note that exhaled aerosols or droplets can be internally generated at different regions of the respiratory system and the droplet size can also vary significantly depending on the source regions (i.e., 1–145 μm) [69].

Only four scenarios of interpersonal short-range airborne transmission were considered in this study. However, there are countless scenarios that can markedly influence the transmission risks. Edmunds et al. summarized such behaviors into four categories, with conversation accounting for 95% of all possible close contact events, i.e., conversation without physical contact (61%) and with physical contact (34%) [70]. Zhang et al. [54] proposed quantitative physical parameters to describe these close contact transmissions, including the two persons' locations and head orientations (1), head/body movement (2), close contact frequency and duration (3), and breathing patterns/intensities (4). So far, the parameters most frequently studied are the interpersonal distance and exposure duration, which have been demonstrated to play an important role in viral transmission [54]. In this study, in addition to the distance and duration, we also observed that the head relative height (i.e., recipient standing and recipient sitting) and face covering type can notably alter the aerosol transmission, including the exposure time for SarGel color change, the variation in deposition with time, and the deposition distribution (Figures 9 and 10). Furthermore, real-life scenarios are often much more complex. An individual changes his/her activity and position throughout the day and may be exposed to varying levels of viral sources. Consequently, the total viral load received by an individual would be an integration of transient exposures over a prescribed period. Future studies are needed to examine how other close-contact parameters influence the transmission risk. Such datasets are vital for creating models of viral spread and planning future outbreak responses.

5. Conclusions

In summary, various visualization methods were attempted to better understand mask flows and interpersonal droplet transmission. Leakage flow velocities at the nose top, two sides, and chin were measured for the cloth, surgical, and KN95 masks, with significant differences among the three masks and between exhalation and inhalation for each mask. Particle counts were measured for five mask types (including neck gaiter and cloth + filter) with a good fit, which were consistent with their filtration efficiency in

comparison to that with no mask. The vapor–SarGel visualization system for interpersonal droplet transmission provided a practical method to simulate the temporospatial transport and deposition of respiratory droplets under varying scenarios or with different face coverings. Significant deposition occurred in the mouth–nose region, as well as in the neck, chin, and jaw, increasing the risk of self-inoculation due to spontaneous face-touching, urging post-exposure hand/face washing. Adding a face shield to a surgical mask notably reduced total droplet deposition on the head and regional deposition in the neck and face, supporting that double face covering can be highly effective when one face covering is deemed inadequate.

Author Contributions: Conceptualization, J.H.P., R.N., X.S. and J.X.; methodology, J.S.X., M.T. and X.S.; software, M.T. and J.X.; validation, J.S.X., J.H.P., R.N., X.S., J.X. and M.R.; formal analysis, J.S.X., M.T. and X.S.; investigation, J.S.X., M.T. and X.S.; Resources: X.S., J.H.P., R.N. and J.X. data curation, M.T.; writing—original draft preparation, J.X.; writing—review and editing, X.S.; visualization, X.S.; supervision, J.X. and M.R. All authors have read and agreed to the published version of the manuscript.

Funding: This study was partially sponsored by the Advanced Functional Fabrics of America and U.S. Army ARDEC under Agreement number W15QKN-16-3-0001.

Institutional Review Board Statement: The study was conducted in accordance with the Declaration of Helsinki, and the protocol was approved by the Ethics Committee of the University of Massachusetts Lowell (protocol code 22-194 and date of approval: 10/02/2022).

Informed Consent Statement: All subjects gave their informed consent for inclusion before they participated in the study.

Data Availability Statement: The data presented in this study are available upon request from the corresponding author.

Acknowledgments: We thank Amr Seifelnasr at UMass Lowell Biomedical Engineering for editing and proofreading this manuscript. Claire Lepont is gratefully acknowledged for the project management.

Conflicts of Interest: The authors declare that they have no known competing financial interests or personal relationships that could have appeared to influence the work reported in this paper. Michael Rein is employee of Advanced Functional Fabrics of America, who has no conflict of interest to declare in this study, and this study received funding from Advanced Functional Fabrics of America and U.S. Army ARDEC. The funder had no role in the design of the study; in the collection, analysis, or interpretation of data, in the writing of the manuscript, or in the decision to publish the results.

References

1. O'Kelly, E.; Arora, A.; Pirog, S.; Ward, J.; Clarkson, P.J. Comparing the fit of N95, KN95, surgical, and cloth face masks and assessing the accuracy of fit checking. *PLoS ONE* **2021**, *16*, e0245688. [CrossRef] [PubMed]
2. Kähler, C.J.; Hain, R. Fundamental protective mechanisms of face masks against droplet infections. *J. Aerosol Sci.* **2020**, *148*, 105617. [CrossRef] [PubMed]
3. Essa, W.K.; Yasin, S.A.; Saeed, I.A.; Ali, G.A.M. Nanofiber-based face masks and respirators as COVID-19 protection: A review. *Membranes* **2021**, *11*, 250. [CrossRef] [PubMed]
4. Yu, B.; Chen, J.; Chen, D.; Chen, R.; Wang, Y.; Tang, X.; Wang, H.-L.; Deng, W. Visualization of the interaction of water aerosol and nanofiber mesh. *Phys. Fluids* **2021**, *33*, 092106. [CrossRef] [PubMed]
5. Shen, H.; Zhou, Z.; Wang, H.; Zhang, M.; Han, M.; Durkin, D.P.; Shuai, D.; Shen, Y. Development of electrospun nanofibrous filters for controlling coronavirus aerosols. *Environ. Sci. Technol. Lett.* **2021**, *8*, 545–550. [CrossRef] [PubMed]
6. Hao, J.; Passos de Oliveira Santos, R.; Rutledge, G.C. Examination of nanoparticle filtration by filtering facepiece respirators during the COVID-19 pandemic. *ACS Appl. Nano Mater.* **2021**, *4*, 3675–3685. [CrossRef]
7. Frankfort, M.G.H.; Lauwers, I.; Pruijn, E.M.C.; Dijkstra, S.F.; Boormans, L.H.G.; Schouten, N.A.; van Donkelaar, C.C.; Janssens, H.M. Minimizing aerosol leakage from facemasks in the COVID-19 pandemic. *J. Aerosol Med. Pulm. Drug Deliv.* **2023**, *36*, 101–111. [CrossRef] [PubMed]
8. Solano, T.; Ni, C.; Mittal, R.; Shoele, K. Perimeter leakage of face masks and its effect on the mask's efficacy. *Phys. Fluids* **2022**, *34*, 051902. [CrossRef]
9. Bradford Smith, P.; Agostini, G.; Mitchell, J.C. A scoping review of surgical masks and N95 filtering facepiece respirators: Learning from the past to guide the future of dentistry. *Saf. Sci.* **2020**, *131*, 104920. [CrossRef]

10. Smith, J.D.; MacDougall, C.C.; Johnstone, J.; Copes, R.A.; Schwartz, B.; Garber, G.E. Effectiveness of N95 respirators versus surgical masks in protecting health care workers from acute respiratory infection: A systematic review and meta-analysis. *Can. Med. Assoc. J.* **2016**, *188*, 567–574. [CrossRef]
11. Lai, A.C.K.; Poon, C.K.M.; Cheung, A.C.T. Effectiveness of facemasks to reduce exposure hazards for airborne infections among general populations. *J. R. Soc. Interface* **2012**, *9*, 938–948. [CrossRef] [PubMed]
12. Lee, L.Y.-K.; Lam, E.P.-W.; Chan, C.-K.; Chan, S.-Y.; Chiu, M.-K.; Chong, W.-H.; Chu, K.-W.; Hon, M.-S.; Kwan, L.-K.; Tsang, K.-L.; et al. Practice and technique of using face mask amongst adults in the community: A cross-sectional descriptive study. *BMC Public Health* **2020**, *20*, 948. [CrossRef] [PubMed]
13. Barnawi, G.M.; Barnawi, A.M.; Samarkandy, S. The association of the prolonged use of personal protective equipment and face mask during COVID-19 pandemic with various dermatologic disease manifestations: A systematic review. *Cureus* **2021**, *13*, e16544. [CrossRef]
14. Ruhle, K.H.; Randerath, W. Measurement of mask leakage during CPAP in patients with obstructive sleep apnea. *Pneumologie* **2000**, *54*, 422–424. [PubMed]
15. Persson, B.N.J. Side-leakage of face mask. *Eur. Phys. J. E. Soft Matter.* **2021**, *44*, 75. [CrossRef]
16. Leidag, M.; Hader, C.; Keller, T.; Meyer, Y.; Rasche, K. Mask leakage in continuous positive airway pressure and C-Flex. *J. Physiol. Pharmacol.* **2008**, *59* (Suppl. 6), 401–406.
17. Mueller, J.T.; Karimi, S.; Poterack, K.A.; Seville, M.T.A.; Tipton, S.M. Surgical mask covering of N95 filtering facepiece respirators: The risk of increased leakage. *Infect. Control Hosp. Epidemiol.* **2021**, *42*, 627–628. [CrossRef]
18. He, X.; Grinshpun, S.A.; Reponen, T.; McKay, R.; Bergman, M.S.; Zhuang, Z. Effects of breathing frequency and flow rate on the total inward leakage of an elastomeric half-mask donned on an advanced manikin headform. *Ann. Occup. Hyg.* **2014**, *58*, 182–194.
19. Crutchfield, C.D.; Park, D.L. Effect of leak location on measured respirator fit. *Am. Ind. Hyg. Assoc. J.* **1997**, *58*, 413–417. [CrossRef]
20. Wang, T.K.; Solano, T.; Shoele, K. Bridge the gap: Correlate face mask leakage and facial features with 3D morphable face models. *J. Expo. Sci. Environ. Epidemiol.* **2022**, *32*, 735–743. [CrossRef]
21. Oestenstad, R.K.; Bartolucci, A.A. Factors affecting the location and shape of face seal leak sites on half-mask respirators. *J. Occup. Environ. Hyg.* **2010**, *7*, 332–341. [CrossRef]
22. Solano, T.; Mittal, R.; Shoele, K. One size fits all?: A simulation framework for face-mask fit on population-based faces. *PLoS ONE* **2021**, *16*, e0252143. [CrossRef] [PubMed]
23. Schmitt, J.; Wang, J. A critical review on the role of leakages in the facemask protection against SARS-CoV-2 infection with consideration of vaccination and virus variants. *Indoor Air* **2022**, *32*, e13127. [CrossRef] [PubMed]
24. Pushpawela, B.; Chea, P.; Ward, R.; Flagan, R.C. Quantification of face seal leakage using parallel resistance model. *Phys. Fluids* **2023**, *35*, 127127. [CrossRef]
25. Larsen, P.S.; Heebøll, J.; Meyer, K.E. Measured air flow leakage in facemask usage. *Int. J. Environ. Res. Public Health* **2023**, *20*, 2363. [CrossRef] [PubMed]
26. Tang, J.W.; Liebner, T.J.; Craven, B.A.; Settles, G.S. A schlieren optical study of the human cough with and without wearing masks for aerosol infection control. *J. R. Soc. Interface* **2009**, *6* (Suppl. 6), S727–S736. [CrossRef] [PubMed]
27. Su, W.C.; Lee, J.; Xi, J.; Zhang, K. Investigation of mask efficiency for loose-fitting masks against ultrafine particles and effect on airway deposition efficiency. *Aerosol Air Qual. Res.* **2022**, *22*, 210228. [CrossRef]
28. Cappa, C.D.; Asadi, S.; Barreda, S.; Wexler, A.S.; Bouvier, N.M.; Ristenpart, W.D. Expiratory aerosol particle escape from surgical masks due to imperfect sealing. *Sci. Rep.* **2021**, *11*, 12110. [CrossRef] [PubMed]
29. Koh, X.Q.; Sng, A.; Chee, J.Y.; Sadovoy, A.; Luo, P.; Daniel, D. Outward and inward protection efficiencies of different mask designs for different respiratory activities. *J. Aerosol Sci.* **2022**, *160*, 105905. [CrossRef]
30. Brooks, J.T.; Beezhold, D.H.; Noti, J.D.; Coyle, J.P.; Derk, R.C.; Blachere, F.M.; Lindsley, W.G. Maximizing fit for cloth and medical procedure masks to improve performance and reduce SARS-CoV-2 transmission and exposure, 2021. *MMWR Morb. Mortal Wkly. Rep.* **2021**, *70*, 254–257. [CrossRef]
31. Verma, S.; Dhanak, M.; Frankenfield, J. Visualizing the effectiveness of face masks in obstructing respiratory jets. *Phys. Fluids* **2020**, *32*, 061708. [CrossRef] [PubMed]
32. Eni, M.; Mordoh, V.; Zigel, Y. Cough detection using a non-contact microphone: A nocturnal cough study. *PLoS ONE* **2022**, *17*, e0262240. [CrossRef] [PubMed]
33. Crawford, F.W.; Jones, S.A.; Cartter, M.; Dean, S.G.; Warren, J.L.; Li, Z.R.; Barbieri, J.; Campbell, J.; Kenney, P.; Valleau, T.; et al. Impact of close interpersonal contact on COVID-19 incidence: Evidence from 1 year of mobile device data. *Sci. Adv.* **2022**, *8*, eabi5499. [CrossRef] [PubMed]
34. Xu, C.; Wei, X.; Liu, L.; Su, L.; Liu, W.; Wang, Y.; Nielsen, P.V. Effects of personalized ventilation interventions on airborne infection risk and transmission between occupants. *Build. Environ.* **2020**, *180*, 107008. [CrossRef] [PubMed]
35. Xu, C.; Nielsen, P.V.; Liu, L.; Jensen, R.L.; Gong, G. Human exhalation characterization with the aid of schlieren imaging technique. *Build. Environ.* **2017**, *112*, 190–199. [CrossRef] [PubMed]
36. Talaat, M.; Barari, K.; Si, X.A.; Xi, J. Schlieren imaging and video classification of alphabet pronunciations: Exploiting phonetic flows for speech recognition and speech therapy. *Vis. Comput. Ind. Biomed. Art* **2024**, *7*, 12. [CrossRef] [PubMed]

37. CDC, NPPTL Respirator Assessments to Support the COVID-19 Response. Available online: https://www.cdc.gov/niosh/npptl/respirators/testing/default.html#:~:text=Workplaces%20should%20make%20every%20effort,Support%20the%20COVID-19%20Response (accessed on 22 June 2024).
38. Forouzandeh, P.; O'Dowd, K.; Pillai, S.C. Face masks and respirators in the fight against the COVID-19 pandemic: An overview of the standards and testing methods. *Saf. Sci.* **2021**, *133*, 104995. [CrossRef] [PubMed]
39. Ranga, U. SARS-CoV-2 aerosol and droplets: An overview. *Virusdisease* **2021**, *32*, 190–197. [CrossRef] [PubMed]
40. Talaat, M.; Si, X.; Xi, J. Breathe out the secret of the lung: Video classification of exhaled flows from normal and asthmatic lung models using CNN-long short-term memory networks. *J. Respir.* **2023**, *3*, 237–257. [CrossRef]
41. April Si, X.; Talaat, M.; Xi, J. SARS-CoV-2 virus-laden droplets coughed from deep lungs: Numerical quantification in a single-path whole respiratory tract geometry. *Phys. Fluids* **2021**, *33*, 023306. [CrossRef]
42. Li, H.; Leong, F.Y.; Xu, G.; Kang, C.W.; Lim, K.H.; Tan, B.H.; Loo, C.M. Airborne dispersion of droplets during coughing: A physical model of viral transmission. *Sci. Rep.* **2021**, *11*, 4617. [CrossRef] [PubMed]
43. Bake, B.; Larsson, P.; Ljungkvist, G.; Ljungström, E.; Olin, A.C. Exhaled particles and small airways. *Respir. Res.* **2019**, *20*, 8. [CrossRef] [PubMed]
44. Xi, J.; Kim, J.; Si, X.A.; Mckee, E.; Corley, R.A.; Kabilan, S.; Wang, S. CFD modeling and image analysis of exhaled aerosols due to a growing bronchial tumor: Towards non-invasive diagnosis and treatment of respiratory obstructive diseases. *Theranostics* **2015**, *5*, 443–455. [CrossRef] [PubMed]
45. Xi, J.; Barari, K.; Si, X.A.; Abdollahzadeh Jamalabadi, M.Y.; Park, J.H.; Rein, M. Inspiratory leakage flow fraction for surgical masks with varying gaps and filter materials. *Phys. Fluids* **2022**, *34*, 041908. [CrossRef]
46. Barari, K.; Si, X.; Xi, J. Impacts of mask wearing and leakages on cyclic respiratory flows and facial thermoregulation. *Fluids* **2024**, *9*, 9. [CrossRef]
47. Xi, J.; Lei, L.R.; Zouzas, W.; April Si, X. Nasally inhaled therapeutics and vaccination for COVID-19: Developments and challenges. *MedComm* **2021**, *2*, 569–586. [CrossRef] [PubMed]
48. Roberge, R.J.; Palmiero, A.J.; Liu, Y.; Kim, J.H.; Zhuang, Z. Effect of upper strap downward displacement on n95 filtering facepiece respirator fit factors: A pilot study. *J. Occup. Environ. Hyg.* **2014**, *11*, 338–341. [CrossRef] [PubMed]
49. South-Shore_Health. How the 'Knot-and-Tuck' Method Achieves a Better Fitting Face Mask. Available online: https://www.southshorehealth.org/wellness/blog/how-knot-and-tuck-method-achieves-better-fitting-face-mask (accessed on 27 May 2024).
50. Cherrie, J.W.; Wang, S.; Mueller, W.; Wendelboe-Nelson, C.; Loh, M. In-mask temperature and humidity can validate respirator wear-time and indicate lung health status. *J. Expo. Sci. Environ. Epidemiol.* **2019**, *29*, 578–583. [CrossRef] [PubMed]
51. Zheng, Z.; Dai, K.; Zhou, X.; Liu, J.; Liu, W.; Lu, J.; Fang, Z. Field investigation of thermal comfort with face masks in outdoor spaces in South China: A case study. *Urban Clim.* **2023**, *51*, 101632. [CrossRef]
52. Hu, R.; Liu, J.; Xie, Y.; Jiao, J.; Fang, Z.; Lin, B. Effects of mask wearing duration and relative humidity on thermal perception in the summer outdoor built environment. *Build. Simul.* **2023**, *16*, 1601–1616. [CrossRef]
53. Oner, E.; Seçkin, A.Ç.; Egeli, D.; Seçkin, M. Investigation of the Thermal Comfort Properties of Masks Used during the COVID-19 Pandemic. *Int. J. Environ. Res. Public Health* **2022**, *19*, 11275. [CrossRef] [PubMed]
54. Zhang, N.; Chen, W.; Chan, P.T.; Yen, H.L.; Tang, J.W.; Li, Y. Close contact behavior in indoor environment and transmission of respiratory infection. *Indoor Air* **2020**, *30*, 645–661. [CrossRef]
55. Xi, J.; Yuan, J.E.; Zhang, Y.; Nevorski, D.; Wang, Z.; Zhou, Y. Visualization and quantification of nasal and olfactory deposition in a sectional adult nasal airway cast. *Pharm. Res.* **2016**, *33*, 1527–1541. [CrossRef] [PubMed]
56. Kwok, Y.L.; Gralton, J.; McLaws, M.L. Face touching: A frequent habit that has implications for hand hygiene. *Am. J. Infect. Control* **2015**, *43*, 112–114. [CrossRef]
57. Chen, Y.J.; Qin, G.; Chen, J.; Xu, J.L.; Feng, D.Y.; Wu, X.Y.; Li, X. Comparison of face-touching behaviors before and during the coronavirus disease 2019 pandemic. *JAMA Netw. Open* **2020**, *3*, e2016924. [CrossRef]
58. Wiener, R.C.; Trickett Shockey, A.K.; Waters, C.; Bhandari, R. Face-touching behavior during the COVID-19 pandemic: Self-inoculation and transmission potentials. *J. Dent. Hyg.* **2021**, *95*, 41–46.
59. Mueller, S.M.; Martin, S.; Grunwald, M. Self-touch: Contact durations and point of touch of spontaneous facial self-touches differ depending on cognitive and emotional load. *PLoS ONE* **2019**, *14*, e0213677. [CrossRef]
60. Rahman, J.; Mumin, J.; Fakhruddin, B. How frequently do we touch facial T-zone: A systematic review. *Ann. Glob. Health* **2020**, *86*, 75. [CrossRef]
61. Nalunkuma, R.; Abila, D.B.; Ssewante, N.; Kiyimba, B.; Kigozi, E.; Kisuza, R.K.; Kasekende, F.; Nkalubo, J.; Kalungi, S.; Muttamba, W.; et al. Double face mask use for COVID-19 infection prevention and control among medical students at Makerere University: A cross-section survey. *Risk Manag. Healthc. Policy* **2022**, *15*, 111–120. [CrossRef]
62. Sickbert-Bennett, E.E.; Samet, J.M.; Prince, S.E.; Chen, H.; Zeman, K.L.; Tong, H.; Bennett, W.D. Fitted filtration efficiency of double masking during the COVID-19 pandemic. *JAMA Intern. Med.* **2021**, *181*, 1126–1128. [CrossRef]
63. Blachere, F.M.; Lemons, A.R.; Coyle, J.P.; Derk, R.C.; Lindsley, W.G.; Beezhold, D.H.; Woodfork, K.; Duling, M.G.; Boutin, B.; Boots, T.; et al. Face mask fit modifications that improve source control performance. *Am. J. Infect. Control* **2022**, *50*, 133–140. [CrossRef] [PubMed]
64. NewYork-Presbyterian. Should You Be Double Masking? Available online: https://healthmatters.nyp.org/should-you-be-double-masking/ (accessed on 27 May 2024).

65. Htwe, Y.Z.N.; Mamat, H.; Osman, B.; Mahmud, H. Performance comparison of single and double masks: Filtration efficiencies, breathing resistance and CO_2 content. *Arab J. Sci. Eng.* **2023**, *48*, 8349–8357. [CrossRef] [PubMed]
66. Patra, S.S.; Nath, J.; Panda, S.; Das, T.; Ramasamy, B. Evaluating the filtration efficiency of commercial facemasks' materials against respiratory aerosol droplets. *J. Air. Waste Manag. Assoc.* **2022**, *72*, 3–9. [CrossRef] [PubMed]
67. Gena, A.W.; Voelker, C.; Settles, G.S. Qualitative and quantitative schlieren optical measurement of the human thermal plume. *Indoor Air* **2020**, *30*, 757–766. [CrossRef] [PubMed]
68. Bridges, J.P.; Vladar, E.K.; Huang, H.; Mason, R.J. Respiratory epithelial cell responses to SARS-CoV-2 in COVID-19. *Thorax* **2022**, *77*, 203–209. [CrossRef] [PubMed]
69. Johnson, G.R.; Morawska, L.; Ristovski, Z.D.; Hargreaves, M.; Mengersen, K.; Chao, C.Y.H.; Wan, M.P.; Li, Y.; Xie, X.; Katoshevski, D.; et al. Modality of human expired aerosol size distributions. *J. Aerosol Sci.* **2011**, *42*, 839–851. [CrossRef]
70. Edmunds, W.J.; Kafatos, G.; Wallinga, J.; Mossong, J.R. Mixing patterns and the spread of close-contact infectious diseases. *Emerg. Themes Epidemiol.* **2006**, *3*, 10. [CrossRef]